Performance evaluation of a naturally ventilated photovoltaic-thermal (PV/T) solar collector: A case study

Amin Shahsavar[1], Pouyan Talebizadeh Sardari[2], Sirous Yasseri[3], Rohollah Babaei Mahani[4]

[1] Department of Mechanical Engineering, Kermanshah University of Technology, Iran.
[2] Faculty of Engineering, University of Nottingham, University Park, Nottingham NG7 2RD, United Kingdom.
[3] Department of Mechanical Engineering, Faculty of Engineering, Brunel University, United Kingdom.
[4] Director, Belmore Energy Ltd., United Kingdom.

Abstract
The objective of this paper is to design and analyze a naturally ventilated photovoltaic-thermal (PV/T) air collector numerically and experimentally in both glazed and unglazed conditions. To reduce the panel's temperature, a thin metal sheet in the middle of the air channel is used to improve thermal and electrical output of the system. A good agreement is first achieved between the numerical results and the measured data. The validated model is then used to evaluate the effective parameters i.e. solar radiation intensity, channel depth and channel length on air mass flow rate, PV cooling, outlet air temperature as well as thermal and electrical efficiencies. The results show that while the thermal efficiency ranges between 12.21-37.17% throughout the day, the electrical efficiency ranges between 3.23-8.12%.

Keywords: Photovoltaic-thermal air collector; Natural convection; Glass cover; Thermal efficiency; Electrical efficiency.

1. Introduction
In hybrid photovoltaic-thermal collectors (PV/T), a combination of both types of thermal collector and the photovoltaic collector is employed to generate thermal and electrical energy simultaneously [1]. The produced electricity can be used to circulate the working liquid through the collector. PV/T systems can generate more energy per unit surface area than single photovoltaic panel due to reduction of PV temperature [2]. Due to the high efficiency of PV/T systems, they are particularly well suited for applications with both heat and power with more advantages for limited available roof space.
PV/T systems has been studied significantly by many researchers both numerically and experimentally. Kern and Russell [3] presented the main concepts of PV/T systems and showed that water or air can be used for removing the heat from the PV panels. Florschuetz [4] developed a linear relationship between the cell efficiency and its operating temperature. Sopian et al. [5] analyzed single and double-pass PV/T air collectors and showed the advantage of double-pass configuration. Moshfegh and Sandberg [6] studied the effect of induced velocity on the reduced heat flux in a naturally ventilated vertical PV/T system. Garg

and Adhikari [7] presented a simulation model for determining the steady-state performance of PV/T air system with single and double glass configurations and showed that the need for glazing depends on the operating temperature. Brinkworth et al. [8] developed a simplified method for calculation of the flow rate in naturally ventilated PV/T integrated in buildings. Sandnes and Rekstad [9] studied hybrid PV/T systems numerically and experimentally and developed an analytical model for flat plate collectors due to the inclusion of additional solar cells. Tripanagnostopoulos et al. [10] investigated thermosyphon-type PV/T systems and showed that, compared to the unglazed systems, glazed PV/T systems for water-heating can improve the thermal efficiency up to 30%; however, the electrical efficiency is reduced by 16%. Chow [11] presented a transient model for a single-glazed sheet-and-tube water-heating PV/T collector which provides the instantaneous thermal/electrical gains and efficiencies, as well as the thermal conditions of the sub-components. Tiwari et al. [12] performed a theoretical and experimental study on a photovoltaic panel integrated with air duct for climate condition of India and concluded that an overall thermal efficiency of PV/T system is significantly increased (18%) due to cooling the PV panel. Tonui and Tripanagnostopoulos [1, 13] investigated a PV/T air system and suggested the use of thin flat metal sheet at the middle or finned back wall of an air channel in the PV/T air configuration to improve the thermal efficiency and cooling the PV panels.

Raman and Tiwari [14, 15] studied a PV/T air collector for five different Indian climate conditions annually. They showed that the energy efficiency is 40-45% lower than the thermal efficiency under high solar radiation intensities. Furthermore, they presented higher advantages of double-pass design than the single-pass configuration. Chow et al. [16] investigated a building-integrated photovoltaic/water-heating system for Hong Kong climates annually and found that the annual thermal and cell conversion efficiencies are 37.5% and 9.39%, respectively. Shahsavar et al. [17] performed a numerical optimization on the performance of PV/T systems based on natural air flow operation using the genetic algorithm in order to find the optimum geometric parameters. Gholampour and Ameri [18] performed an exergy and energy analysis of a naturally ventilated PV/T with the aid of fins for heat transfer enhancement to the air and temperature reduction of the PV. Guarracino et al. [19] developed a dynamic model for PV/T collectors with a sheet-and-tube thermal absorber in order to generate electricity and domestic hot water, simultaneously as well as reducing the PV temperature.

In this study, a naturally ventilated PV/T air collector is designed, built and tested at a geographic location of Kerman, Iran. In this system, a thin metal sheet is used to improve heat extraction from the panels to reduce the temperature and consequently achieving higher thermal and electrical output. The metal sheet is suspended in the middle of an air channel in the studied PV/T air system. The objective of this paper is to study the performance of this system for both glazed and unglazed types.

2. Experimental setup

The cross-sectional schematic view of the studied PV/T air collector is shown in Figure 1a and a picture of the setup is displayed in Figure 1b.

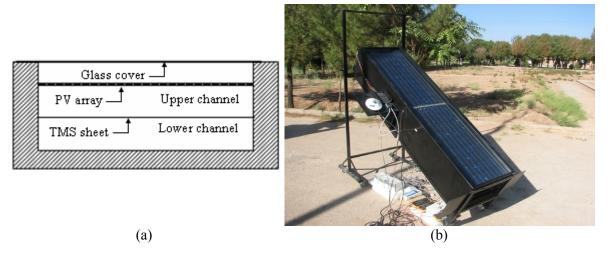(a)   (b)

Figure 1. The studied PV/T air collector (a) a Cross-sectional schematic view; (b) Photograph of experimental setup.

The basic components of the system are as follows:
- Two polycrystalline silicon type PV panels, each rated at 45 W peak having length, width, and height 0.98, 0.46, and 0.04 m, respectively.
- The air channel constructed from wood with dimensions of $1.96 \times 0.54 \times 0.35$ m.
- A thin metal sheet (TMS) with the material of Aluminum suspended at the middle of air channel.
- Two lamps of 35W, as a resistive load.
- 5 mm-thick glass cover for the glazed configuration.
- 25 mm-thick fibreglass for insulation of the channel walls.

The channel walls and the metal sheet are black to increase their absorptivity and emissivity. Furthermore, the PV array with wooden structure and is tilted at 30° (equal to the latitude of Kerman) to maximize the solar energy gain [20, 21].

Since the system is naturally ventilated, the driving force in the air channel is the buoyancy force that controls the induced flow rate. Note that the local wind is neglected in this study. The opposing forces are the frictional losses between channel walls and the airflow as well as the pressure gradients created at the entrance, the exit and any control device in the flow channel.

According to the Iranian meteorological organization (IMO), the annual solar radiation in Kerman is about 7625 MJ/m². Since Kerman has a high irradiation level, a considerable amount of its energy requirements may be obtained from solar energy systems such as photovoltaic panels [20].

2.1 Measurements
The following parameters are measured in the experiments:
- Velocity of the air flowing through upper (v_{f1}) and lower (v_{f2}) channels.

- Load current (I_l) and load voltage (V_l).

- Temperature of ambient air (T_a), the PV panels (T_{pv}), TMS sheet (T_{TMS}), back insulation wall (T_b) as well as outlet air from upper (T_{f1}) and lower (T_{f2}) channels.

- Solar radiation Intensity (I_r).

- Wind speed (v_w).

A digital Testo 405-V1 thermometer is used for measuring the ambient air temperature. The thermometer is located outside about 1.5 m above the ground. The device is also used for measuring the speed of air stream in the upper and lower channels. Type PT100 thermocouples are used for the temperature measurement. A BM 6 Kipp & Zonen pyranometer is used for measuring the incident solar intensity on the PV panels and an NRG40 anemometer is used to record the wind speed. The pyranometer is mounted on the surface parallel to the collector surface in such a manner that is would not cast a shadow onto the collector plate. Two DT-9205 type multimeters are used for measuring voltage and current of PV panels and the resistive load. The experimental results for a typical two days in the month of July 2009 for Kerman condition are shown in Tables 1 and 2 for glazed and unglazed types, respectively.

Table 1. Observation obtained for glazed type.

Time	$I_r(W/m^2)$	$T_a(°C)$	$T_{pv}(°C)$	$T_{f1}(°C)$	$T_{f2}(°C)$	$V_l(V)$	$I_l(A)$	$v_{f1}(m/s)$	$v_{f2}(m/s)$
10:00	641	30.2	57	37.8	36	7.58	2.32	0.32	0.15
10:30	727	31.4	60.3	40.6	37.8	10.85	2.95	0.29	0.23
11:00	792	32	63.4	42.5	40.5	12.8	3.27	0.29	0.16
11:30	816	33.2	67	43.9	41	12.9	3.31	0.31	0.11
12:00	864	34.3	68.7	45.4	42.3	13.08	3.32	0.33	0.12
12:30	884	34.6	70.6	45.8	42.5	12.97	3.33	0.33	0.12
13:00	880	34.8	70.8	46.8	42.5	13.12	3.29	0.34	0.12
13:30	870	36.1	70.2	48.3	42.5	13	3.25	0.36	0.07
14:00	846	36	71.1	46.8	43.5	12.85	3.19	0.32	0.12
14:30	800	36.5	70.8	47.3	44.7	10.56	2.86	0.32	0.13
15:00	725	35.6	68.8	45.8	44.1	9.62	2.67	0.29	0.16

Table 2. Observation obtained for unglazed type.

Time	$I_r(W/m^2)$	$T_a(°C)$	$T_{pv}(°C)$	$T_{f1}(°C)$	$T_{f2}(°C)$	$V_l(V)$	$I_l(A)$	$v_{f1}(m/s)$	$v_{f2}(m/s)$
10:00	650	30.8	48.4	39.3	37.7	10.84	2.89	0.16	0.08
10:30	732	32.4	53.2	40.7	39.7	14.39	3.51	0.14	0.1
11:00	799	32.7	54.8	41.4	40.3	14.88	3.58	0.18	0.11
11:30	848	34.7	59.1	43.4	42.1	14.85	3.57	0.18	0.1
12:00	889	34.7	60.5	43.5	42.8	14.96	3.59	0.18	0.12
12:30	899	35.4	60.9	44.4	43.3	14.95	3.55	0.23	0.12
13:00	899	35.8	61.1	46.3	43.9	14.83	3.54	0.2	0.1
13:30	880	36.6	62.5	46.8	44.1	14.7	3.46	0.29	0.12
14:00	848	37.4	62.6	47.5	44.4	14.58	3.5	0.29	0.09
14:30	794	36.4	60.5	45.6	44.5	14.38	3.5	0.24	0.12
15:00	731	36.3	57.5	45.3	44.3	13.72	3.4	0.23	0.12

2.2 Air mass flow rate

The mass flow rate of flowing air in the upper and lower channels of the studied PV/T system can be calculated as [1]:

$$\dot{m} = \left(\frac{2g\beta(A_{ch}\rho)^2 A_{ch}\eta_{th}I_r L\sin\theta}{C_p(fL/D_H + 2\beta T_{out})} \right)^{\frac{1}{3}} \tag{1}$$

where A_{ch} is the channel area, ρ is the air density, θ is the collector tilt angle, η_{th} is the thermal efficiency of the system, and f is the friction factor that is calculated from the equation given by Tsuji and Nagano [22] for laminar (Eq. (2)) and turbulent (Eq. (3)) flow as:

$$f = 1.906(Gr/Pr)^{1/12} \tag{2}$$

$$f = 1.368(Gr/Pr)^{1/11.9} \tag{3}$$

D_H is the hydraulic diameter of the channel given as [23]:

$$D_H = \frac{4A_{ch}}{P} \tag{4}$$

where A_{ch} and P are the cross-sectional area and the wetted perimeter of the channel, respectively.

2.3 Energy balance equations

Figure 2 shows the studied PV/T collector indicating heat transfer coefficients for different parts.
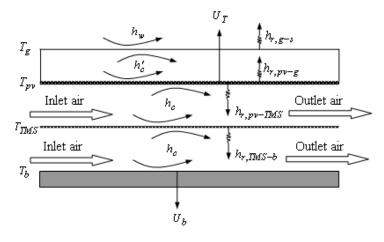

Figure 2. Schematic of the studied PV/T air system with heat transfer coefficients.

The following assumptions are considered to drive the energy balance analysis [24]:
- One-dimensional steady-state heat transfer.
- Negligible thermal capacities of the system components except for the flowing air.
- Equal convection heat transfer coefficient between the channel surfaces, the metal sheet, and the flowing air.
- Uniform temperatures of the PV panels, TMS sheet, glass cover and the back insulation surface.

Therefore, the energy balance equations for the different components of the system are given as:
- Glass cover

$$\alpha_g I_r w dx = (h_{r,pv-g} + h'_c)(T_g - T_{pv})w dx + (h_{r,g-s} + h_w)(T_g - T_a)w dx \tag{5}$$

- PV panel

$$\tau_g \alpha_{pv}(1 - \eta_c) I_r w dx = U_T(T_{pv} - T_a)w dx + h_c(T_{pv} - T_{f1})w dx$$
$$+ h_{r,pv-TMS}(T_{pv} - T_{TMS})w dx \tag{6}$$

- Upper channel air stream

$$\dot{m}_{f1} C_p dT_{f1} = h_c(T_{pv} - T_{f1})w dx + h_c(T_{TMS} - T_{f2})w dx \tag{7}$$

- TMS sheet

$$h_{r,pv-TMS}(T_{pv} - T_{TMS})w dx = h_c(T_{TMS} - T_{f1})w dx + h_c(T_{TMS} - T_{f2})w dx$$
$$+ h_{r,TMS-b}(T_{TMS} - T_b)w dx \tag{8}$$

- Lower channel air stream

$$\dot{m}_{f2} C_p dT_{f2} = h_c(T_{TMS} - T_{f2})w dx + h_c(T_b - T_{f2})w dx \tag{9}$$

- Back insulation surface

$$h_{r,TMS-b}(T_{TMS} - T_b)w dx = U_b(T_b - T_a)w dx + h_c(T_b - T_{f2})w dx \tag{10}$$

For unglazed type, Eq. (5) is transformed to the following equation:

$$\alpha_{pv}(1 - \eta_c) I_r w dx = (h_w + h_{r,pv-s})(T_{pv} - T_a)w dx + h_c(T_{pv} - T_{f1})w dx$$
$$+ h_{r,pv-TMS}(T_{pv} - T_{TMS})w dx \tag{11}$$

Equations (6) to (10) can be combined to give the following two differential equations:

$$\frac{dT_{f1}}{dx} = \alpha_1 T_{f1} + \alpha_2 T_{f2} + \alpha_3 \tag{12}$$

$$\frac{dT_{f2}}{dx} = \beta_1 T_{f1} + \beta_2 T_{f2} + \beta_3 \tag{13}$$

The boundary conditions are as follows:

$$T_{f1}(x = 0) = T_{f2}(x = 0) = T_a \tag{14}$$

Hence, the two differential equations to find the air outlet temperatures are solved numerically using the Runge-Kutta method in this paper.

2.4 Heat transfer coefficients

2.4.1 Heat loss coefficients

The PV loss coefficient from the PV panels to the ambient air via the front glazing can be determined as [25]:

$$U_T = \left[\frac{N}{(C/T_{pv})[(T_{pv}-T_a)/(N+q)]^e} + \frac{1}{h_w} \right]^{-1} +$$

$$\left[\frac{(\varepsilon_{pv}+0.00591N.h_w)^{-1}+[(2N+q-1+0.133\varepsilon_{pv})/\varepsilon_g]-N}{\sigma(T_{pv}+T_a)(T_{pv}^2+T_a^2)} \right]^{-1} \tag{15}$$

where c, e and q are defined as:

$$c = 520(1-0.000051\theta^2) \quad for \quad 0° < \theta < 70°$$
$$\theta = 70° \quad if \quad 70° < \theta < 90° \tag{16}$$

$$e = 0.43(1-\frac{100}{T_{pv}}) \tag{17}$$

$$q = (1+0.089h_w-0.1166h_w\varepsilon_{pv})(1+0.07866N) \tag{18}$$

The wind convection heat transfer coefficient is defined as [26]:

$$h_w = 2.8 + 3v_w \tag{19}$$

The loss coefficient from the bottom accounts for the conduction losses through the back insulation of the solar collector which is given by:

$$U_b = \frac{k_{ins}}{\delta_{ins}} \tag{20}$$

where k_{ins} and δ_{ins} are the thermal conductivity and thickness of the insulation material.

2.4.2 Convection heat transfer coefficients

The free convection heat transfer coefficient of the air gap of height $s = 25$ mm between the PV panels and glass cover is calculated from the equation derived by Hollands et al. [27, 28] as:

$$h'_c = k/s\left\{1+1.44[1-R]^*(1-R(\sin1.8\theta)^{1.6})+[0.66416R^{-1/3}-1]^*\right\} \tag{21}$$

where $R = 1708/Ra_s\cos\theta$ and Ra_s is the air gap Rayleigh number ($= \frac{L^3.g.\sin\theta.\beta.\Delta T}{v.\alpha}$, ΔT is the temperature difference between the PV surface and the glass cover). The notation $[\ ]^*$ means that if those parameters become negative they should be replaced by zero. All above properties are calculated for the mean temperature, $(T_{pv}+T_g)/2$.

The natural convection heat transfer coefficients between the airflow and both the PV panels and the TMS sheet as the back wall are calculated as [29]:

$$h_c = \frac{k}{D_H}\left(0.0965Ra^{0.29}\right) \tag{22}$$

where k is the thermal conductivity of air.

2.4.3 Radiation heat transfer coefficient

The radiative heat transfer coefficient between the glass cover and the sky is defined as [26]:

$$h_{r,g-s} = \sigma \, \varepsilon_g \, \frac{(T_g^4 - T_s^4)}{T_g - T_a} \tag{23}$$

With subscript g is replaced by pv for the unglazed type.
The equivalent sky temperature is evaluated as [26]:

$$T_s = 0.0552 T_a^{1.5} \tag{24}$$

The radiative heat transfer coefficient in the air cavities is determined using the linearized coefficient from Stefan-Boltzmann equation [26]:

$$h_{r,1-2} = \sigma(T_1 + T_2)(T_1^2 + T_2^2)\left(\frac{1}{\varepsilon_1} + \frac{1}{\varepsilon_2} - 1\right)^{-1} \tag{25}$$

where, the subscripts 1 and 2 represent any two surfaces seeing each other.

2.5 Calculation of the current and voltage of the resistive load

Figure 3 is an equivalent circuit used either for an individual cell, a panel consisting of several cells or for an array consisting of several panels.
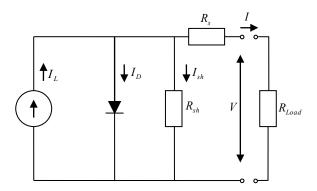

Figure 3. The equivalent circuit for a PV generator.

The relationship between current and voltage is given as [26]:

$$I = I_L - I_D - I_{sh} = I_L - I_o \left\{ \exp\left[(V + I.R_s)/a\right] - 1 \right\} - \frac{V + I.R_s}{R_{sh}} \tag{26}$$

where I_L is the light current in (A), I_D is the diode current of the equivalent circuit in (A), I_o is the inverse polarization current in (A), R_s is the series resistance in (Ω), R_{sh} is the shunt resistance in (Ω), and a is the curve fitting parameter. Rauschenbach [30] showed that the shunt resistance of most modern cells is very large and therefore the last term of Eq. (26) can be neglected. Therefore Eq. (26) can be reduced to:

$$I = I_L - I_D - I_{sh} = I_L - I_o \left\{ \exp\left[(V + I.R_s)/a\right] - 1 \right\} \tag{27}$$

where: I_L, I_o, R_s and a depend on the solar radiation and the temperature of the PV panel [26] based on information for I and V given by the manufacturer of a PV unit for reference solar radiation, I_{ref}, at a reference temperature, T_{ref}, (Table 3), and are described as [26]:

$$I_{L,ref} = I_{sc,ref} \tag{28}$$

$$a_{ref} = \frac{\mu_{V,oc}T_{c,ref} - V_{oc,ref} + \varepsilon N_s}{\dfrac{\mu_{I,sc}T_{c,ref}}{I_{L,ref}} - 3} \tag{29}$$

$$R_{s,ref} = \frac{a_{ref}\ln\left(1 - \dfrac{I_{mp,ref}}{I_{L,ref}}\right) - V_{mp,ref} + V_{oc,ref}}{I_{mp,ref}} \tag{30}$$

$$I_{o,ref} = \frac{I_{L,ref}}{\exp(V_{oc,ref}/a_{ref}) - 1} \tag{31}$$

Table 3. Nominal and reference parameters of PV units.

$N_s = 36$ cells	$I_{sc,ref} = 2.98A$	$I_{mp,ref} = 2.76A$	$\mu_{I,sc} = 1.325mA/K$	$T_{a,ref} = 298K$
$P_{max} = 45W$	$V_{oc,ref} = 20.5V$	$V_{mp,ref} = 16.3V$	$\mu_{V,oc} = -0.0775V/K$	$I_{r,ref} = 1000W/m^2$

The subscripts oc, sc, mp and ref refer to open circuit, short circuit, maximum power, and reference conditions, respectively. ε is the energy gap of silicon (1.12 eV), N_s is the number of cells connected in series in a single unit of the PV system, and $\mu_{V_{oc}}$, $\mu_{I_{sc}}$ are the temperature coefficients of the open circuits voltage and closed circuits current, respectively. The mentioned parameters vary by different solar radiation intensities and temperature conditions based on the following equations:

$$\frac{a}{a_{ref}} = \frac{T_{pv}}{T_{pv,ref}} \tag{32}$$

$$I_L = \frac{I_r}{I_{r,ref}}\left[I_{L,ref} + \mu_{I,sc}(T_{pv} - T_{c,ref})\right] \tag{33}$$

$$\frac{I_o}{I_{o,ref}} = \left(\frac{T_{pv}}{T_{pv,ref}}\right)^3 \exp\left[\frac{\varepsilon N_s}{a_{ref}}\left(1 - \frac{T_{pv,ref}}{T_{pv}}\right)\right] \tag{34}$$

$$R_s = R_{s,ref} \tag{35}$$

In brief, the evaluation of the characteristic equation of a PV panel is as follows: first, Eqs. (28) to (31) are used to estimate the values of the four parameters at reference conditions. Next, these values are adjusted to the actual operating conditions with Eqs. (32) to (35). Finally, the system current, I, is calculated from Eq. (36) which is derived from Eq. (27) accounting for the PV panels that are connected in parallel (NP) and in series (NS) [26]:

$$I = NP.I_L - NP.I_o\left[\exp\left(\frac{V + I.\dfrac{NS}{NP}.R_s}{NS.a}\right) - 1\right] \tag{36}$$

while the $I-V$ curve of a resistance is described by Ohms law:

$$V_l = I_l.R_l \tag{37}$$

where R_l is the resistance. At any time, the combination of the PV panels and the resistive load will operate at the intersection of the characteristic curves of the two components.

2.6 Evaluation of the performance parameters
The conversion efficiency, η_c of the PV panel, is formulated as a function of its temperature T_{pv} given as [4]:

$$\eta_c = \eta_{ref}(1 - \beta_{ref}(T_{pv} - T_{ref})) \tag{38}$$

where β_{ref} is the temperature coefficient of solar cell efficiency and η_{ref} is the panel efficiency at the reference temperature T_{ref}. The values of η_{ref} were found experimentally as 0.132 and 0.125 for unglazed and glazed systems respectively with $T_{ref} = 25\ °C$ while β_{ref} was obtained as 0.006 $°C^{-1}$ for both types. Three kinds of efficiencies are defined for a PV/T collector. The thermal efficiency is defined as:

$$\eta_{th} = \frac{\dot{m}c_p(T_{out} - T_{in})}{I_r.A_{pv}} \tag{39}$$

The electrical efficiency depends mainly on the incoming solar radiation, the temperature of the PV panels and resistive loads consumed power. The electrical efficiency of the system is defined as:

$$\eta_{el} = \frac{I_l.V_l}{I_r.A_{pv}} \tag{40}$$

where I_l and V_l are the current and voltage of the resistive load.
Finally, the total efficiency of the studied PV/T air collector is calculated by [2, 7, 31]:

$$\eta_{tot} = \eta_{th} + \eta_{el} \tag{41}$$

3. Results and discussion
3.1 Validation of the model
Figures 4 to 6 show the comparison between experimental and theoretical values of the temperatures of the outlet air and PV panels as well as the air mass flow rate for both glazed and unglazed types. Note that the measured weather data presented in Tables 1 and 2 are used as the input data of the numerical code. As shown, a good agreement can be seen between the theoretical and experimental values.
Furthermore, the glazed type has a higher PV temperature than unglazed configuration since the glazing increases the operating temperature of the system [7]. Increasing the PV temperature leads to a higher the buoyancy force and consequently increases the air mass flow rate through the channel. Therefore, it is concluded that the glazed type has a higher value of air mass flow rate than unglazed type as shown in Figure 6.
Comparisons between operating voltage and current of the PV panels and resistive load are presented in Figures 7 and 8 for both glazed and unglazed types, respectively. It is obvious from these figures that unglazed system has higher values of the voltage and current than glazed type. This is due to the lower PV temperature hence higher performance of the PV panels. Also, there is a quite good agreement between measured and predicted values of the voltage and current.
Figures 9 to11 show the hourly variation of the thermal, electrical, and total efficiency for glazed and unglazed systems, respectively. It is found that there is a good agreement between the experimental and theoretical results. The thermal efficiency ranges between 12.21-37.17% throughout the day whereas electrical efficiency ranges between 3.23-8.12%. The total efficiency is of the order of 20.33-42.44%. Furthermore, setting the glass cover on the photovoltaic panels leads to an increase in thermal efficiency

and a reduction of electrical efficiency of the system. Therefore, it is concluded that using glass cover is suitable just in the application that thermal efficiency has a more priority than electrical efficiency.
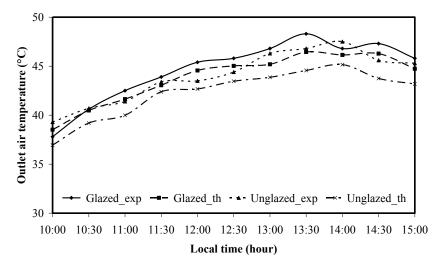

Figure 4. Comparison of experimental and theoretical outlet air temperature for both glazed and unglazed types.
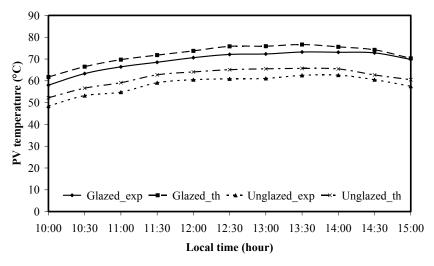

Figure 5. Comparison of experimental and theoretical PV panel temperature for both glazed and unglazed types.
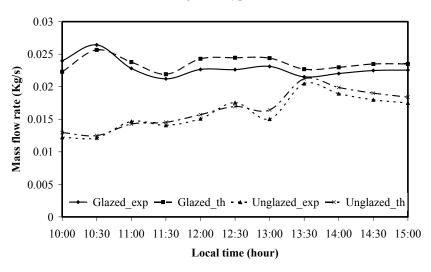

Figure 6. Comparison of experimental and theoretical air mass flow rate for both glazed and unglazed types.
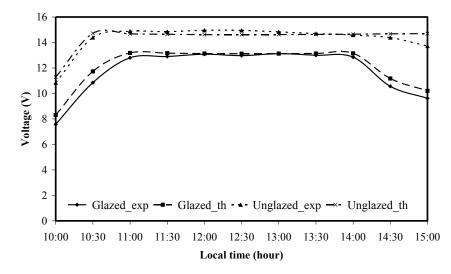
Figure 7. Comparison of experimental and theoretical operating voltage of the PV panels for both glazed and unglazed types.
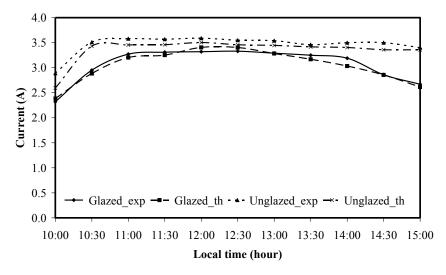

Figure 8. Comparison of experimental and theoretical operating current of the PV panels for both glazed and unglazed types.
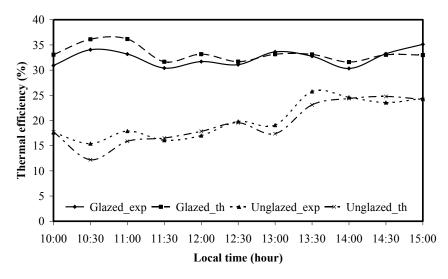

Figure 9. Comparison of experimental and theoretical thermal efficiency for both glazed and unglazed types.
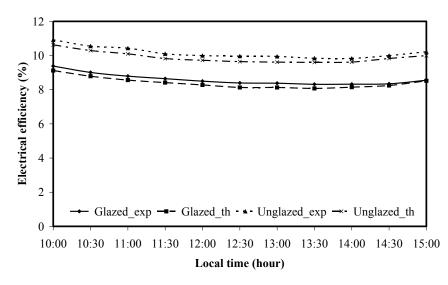
Figure 10. Comparison of experimental and theoretical electrical efficiency for both glazed and unglazed types.
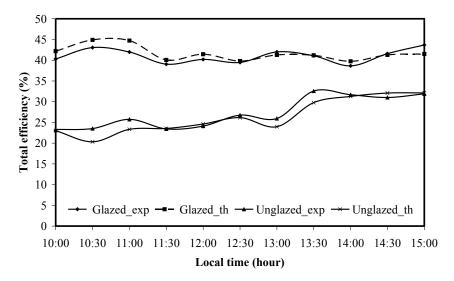

Figure 11. Comparison of experimental and theoretical total efficiency for both glazed and unglazed types.
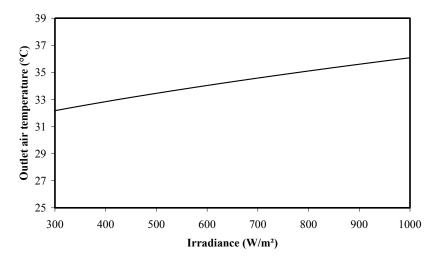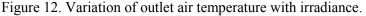
3.2 Case studies
In this section, the validated model is used to study the effects of the incident solar radiation, channel depth and channel length on the air mass flow rate, temperatures of the PV panels and outlet air as well as thermal and electrical efficiencies of the studied PV/T collector. Note that the irradiance and wind speed are considered 800 W m^{-2} and 1.5 ms^{-1}, respectively and the ambient and inlet air temperatures is also 25 °C.

3.2.1 Effect of incident solar radiation
In natural flow systems, the air velocity depends on the heat flux, which is represented by the incident solar radiation absorbed by the PV/T panels. Figures 12-14 give the effect of the solar radiation intensity on the outlet air temperature, PV panel temperature and air mass flow rate, respectively. It is seen that both temperatures and air mass flow rate increase with increasing solar radiation intensity. As shown, the results for both glazed and unglazed systems are the same except that for the glazed systems are slightly elevated than the unglazed systems due to higher temperatures of operation and the results for glazed systems are presented here.

With increasing the solar radiation, the air mass flow rate increases due to more irradiance intercepted by the PV/T collector. Therefore, more heat energy is gained by air in the channel increasing the temperature in the outlet and creating a higher stack effect.
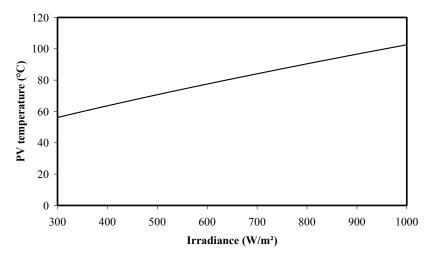
Figure 12. Variation of outlet air temperature with irradiance.

Figure 13. Variation of PV panel temperature with irradiance.

Figure 14. Variation of air mass flow rate with irradiance.

3.2.2 Effect of channel depth

Figure 15 illustrates the effect of the channel depth on the outlet air and PV panel temperature. It is seen that the outlet air temperature decreases with channel depth while the PV panel temperature increases with the channel depth. This is due to the variation of air velocity and convection heat transfer coefficient with the channel depth where both quantities decrease with increasing channel depth.

Figure 16 illustrates the effect of channel depth on the thermal efficiency, where it is clear that the thermal efficiency decreases with increasing the channel depth due to a decrease in the outlet air temperature. The variation of the electrical efficiency with channel depth is illustrated in Figure 17. As shown, the electrical efficiency reduces with increasing channel depth. This is attributed to the increased PV temperature that leads to a decrease in the resistive load's consumed power.
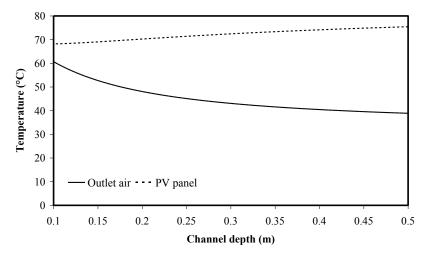

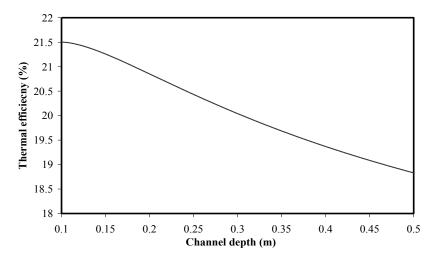Figure 15. Effect of channel depth on the outlet air and PV panel temperature.

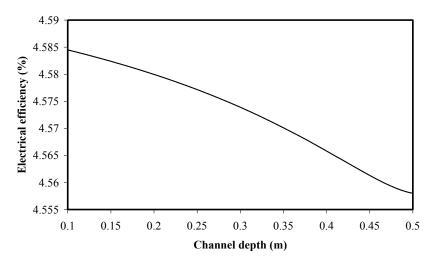Figure 16. Effect of channel depth on the thermal efficiency.

Figure 17. Effect of channel depth on the electrical efficiency.

3.2.3 Effect of channel length

Figure 18 displays the effect of the channel length on the thermal and electrical efficiency, respectively. The thermal efficiency increases and the electrical efficiencies decreases with the channel length. A higher collector length increases the collection area and therefore more solar radiation is intercepted which gives more energy to airflow which results in a higher thermal efficiency. On the other hand, a higher collector length leads to a higher PV panel temperature leading to the reduction in the electrical efficiency as the channel length increases.
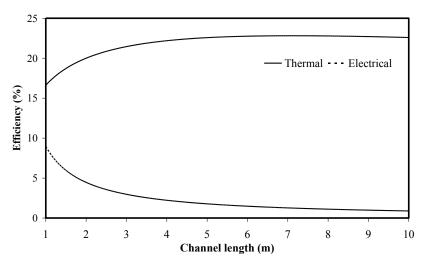

Figure 18. Effect of channel length on the thermal and electrical efficiency.

4. Conclusion

Theoretical and experimental studies of a naturally ventilated PV/T air collector was conducted in this paper. Based on the presented results, the following conclusions were achieved:

- There is a good agreement between the predicted and measured results.
- The thermal efficiency ranges between 12.21-37.17% throughout the day whereas electrical efficiency ranges between 3.23-8.12%. The total efficiency is of the order of 20.33-42.44%.
- Setting glass cover on photovoltaic panels leads to a higher thermal efficiency and a lower electrical efficiency. Therefore, using glass cover is suitable when the thermal efficiency has a higher priority than electrical efficiency.
- The outlet air and the PV panel temperatures as well as the air mass flow rate increase with increasing the solar radiation intensity.
- The outlet air temperature, the thermal efficiency, and the electrical efficiency reduce with increasing the channel depth, while the PV temperature increases with increasing the channel depth.
- The outlet air temperature increases with increasing the channel length, as a result the thermal efficiency increases. On the other hand, increasing the channel length results in higher PV temperature causing the reduction in electrical efficiency as the collector length increases.

Nomenclature

A_{ch} the cross-sectional area of the channel (m^2)

A_{pv} PV array aperture area (m^2)

C_p specific heat capacity of air (J Kg^{-1} K^{-1})

D_H hydraulic diameter (m)

f friction factor

g acceleration due gravity (ms^{-2})

Gr Grashof number

h_c convection heat transfer coefficient in the air channel (WK^{-1} m^{-2})

h_c' convection heat transfer coefficient from PV to glass cover (WK^{-1} m^{-2})

$h_{r,g-s}$ radiation heat transfer coefficient between glass cover and sky (WK^{-1} m^{-2})

$h_{r,pv-g}$	radiation heat transfer coefficient between PV and glass cover (WK^{-1} m^{-2})
$h_{r,pv-TMS}$	radiation heat transfer coefficient between PV and TMS sheet (WK^{-1} m^{-2})
$h_{r,TMS-b}$	radiation heat transfer coefficient between TMS sheet and back insulation wall (WK^{-1} m^{-2})
h_w	wind convection heat transfer coefficient (WK^{-1} m^{-2})
I	the operating current of PV array (A)
I_D	diode current (A)
I_L	light current (A)
I_l	operating current of resistive load (A)
I_{mp}	the operating current of PV panel at maximum power point condition (A)
I_o	inverse polarization current (A)
I_{oc}	open circuit current (A)
I_r	solar radiation intensity (Wm^{-2})
I_{sc}	short circuit current (A)
k	the thermal conductivity of air (Wm^{-1} K^{-1})
k_{ins}	the thermal conductivity of insulation material (Wm^{-1} K^{-1})
L	length of the collector (m)
$\dot{m}$	the total mass flow rate of air flowing through system channels (Kgs^{-1})
$\dot{m}_{f1}$	mass flow rate of air flowing through the upper channel (Kgs^{-1})
$\dot{m}_{f2}$	mass flow rate of air flowing through the lower channel (Kgs^{-1})
N	number of the glass cover
NP	number of PV panels connected in parallel
NS	number of PV panels connected in series
P	the wetted perimeter of the channel
Pr	Prandtl number
R_l	resistance (Ω)
Ra	Rayleigh number
R_s	series resistance (Ω)
R_{sh}	shunt resistance (Ω)
s	the height of air gap between PV and glass cover (m)
T_a	ambient temperature (°C)
T_b	back wall temperature (°C)
T_g	glass cover temperature (°C)
T_{out}	outlet air temperature (°C)
T_{pv}	PV temperature (°C)
T_{TMS}	TMS sheet temperature (°C)
U_b	back heat loss coefficient (WK^{-1} m^{-2})
U_T	top heat loss coefficient (WK^{-1} m^{-2})
v_{f1}	the velocity of air flowing through the upper channel (ms^{-1})
v_{f2}	the velocity of air flowing through the lower channel (ms^{-1})
V	operating voltage of PV panel (V)
V_l	operating voltage of PV array and resistive load (V)
V_{mp}	operating voltage of PV panel at maximum power point condition (V)
V_{oc}	open circuit voltage (V)
V_{sc}	short circuit voltage (V)
v_w	wind velocity (ms^{-1})
w	the width of the collector (m)

Greek symbols

α	thermal diffusivity (m^2 s^{-1})
α_g, α_{pv}	absorptance of glass cover and PV cells, respectively
β	thermal expansivity of air (K^{-1})
β_{ref}	temperature coefficient of PV cells ($^\circ C^{-1}$)
$\varepsilon_g, \varepsilon_{pv}$	the emissivity of glass cover and PV cells, respectively
θ	collector tilt angle
η_c	PV panel electrical efficiency at T_{pv}
η_{ref}	PV panel electrical efficiency at reference temperature
η_{el}	electrical efficiency
η_{th}	thermal efficiency
η_{tot}	total efficiency
ρ	density (Kg m^{-3})
ν	kinematic viscosity (m^2 s^{-1})
σ	Stefan-Boltzmann constant (5.67×10^{-8} W m^{-2} K^{-4})
τ_g	the transmittance of the glass cover
δ_{ins}	the thickness of insulation material (m)
$\mu_{I,sc}$	temperature coefficients of the short circuits current (A K^{-1})
$\mu_{V,oc}$	temperature coefficients of the open circuits voltage (V K^{-1})

References

[1] J.K. Tonui, Y. Tripanagnostopoulos, Performance improvement of PV/T solar collectors with natural air flow operation, Solar Energy, 82 (2008) 1-12.

[2] T. Fujisawa, T. Tani, Binary utilization of solar energy with photovoltaic-thermal hybrid collector, in: ISES Solar World Congress, Taejon, Korea, 1997, pp. 24-30.

[3] E. Kern Jr, M. Russell, Combined photovoltaic and thermal hybrid collector systems, in, Massachusetts Inst. of Tech., Lexington (USA). Lincoln Lab., 1978.

[4] L. Florschuetz, Extension of the Hottel-Whillier model to the analysis of combined photovoltaic/thermal flat plate collectors, Solar Energy, 22 (1979) 361-366.

[5] K. Sopian, K. Yigit, H. Liu, S. Kakac, T. Veziroglu, Performance analysis of photovoltaic thermal air heaters, Energy Conversion and Management, 37 (1996) 1657-1670.

[6] B. Moshfegh, M. Sandberg, Investigation of fluid flow and heat transfer in a vertical channel heated from one side by PV elements, part I-Numerical Study, Renewable Energy, 8 (1996) 248-253.

[7] H. Garg, R. Adhikari, Conventional hybrid photovoltaic/thermal (PV/T) air heating collectors: steady-state simulation, Renewable Energy, 11 (1997) 363-385.

[8] B. Brinkworth, R. Marshall, Z. Ibarahim, A validated model of naturally ventilated PV cladding, Solar Energy, 69 (2000) 67-81.

[9] B. Sandnes, J. Rekstad, A photovoltaic/thermal (PV/T) collector with a polymer absorber plate. Experimental study and analytical model, Solar Energy, 72 (2002) 63-73.

[10] Y. Tripanagnostopoulos, T. Nousia, M. Souliotis, P. Yianoulis, Hybrid photovoltaic/thermal solar systems, Solar Energy, 72 (2002) 217-234.

[11] T. Chow, Performance analysis of photovoltaic-thermal collector by explicit dynamic model, Solar Energy, 75 (2003) 143-152.

[12] A. Tiwari, M. Sodha, A. Chandra, J. Joshi, Performance evaluation of photovoltaic thermal solar air collector for composite climate of India, Solar Energy Materials and Solar Cells, 90 (2006) 175-189.

[13] J. Tonui, Y. Tripanagnostopoulos, Air-cooled PV/T solar collectors with low cost performance improvements, Solar Energy, 81 (2007) 498-511.

[14] V. Raman, G. Tiwari, Life cycle cost analysis of HPVT air collector under different Indian climatic conditions, Energy Policy, 36 (2008) 603-611.

[15] V. Raman, G. Tiwari, A comparison study of energy and exergy performance of a hybrid photovoltaic double-pass and single-pass air collector, International Journal of Energy Research, 33 (2009) 605-617.

[16] T.T. Chow, G. Pei, K. Fong, Z. Lin, A. Chan, J. Ji, Energy and exergy analysis of photovoltaic–thermal collector with and without glass cover, Applied Energy, 86 (2009) 310-316.

[17] A. Shahsavar, P. Talebizadeh, H. Tabaei, Optimization with genetic algorithm of a PV/T air collector with natural air flow and a case study, Journal of Renewable and Sustainable Energy, 5 (2013) 023118.

[18] M. Gholampour, M. Ameri, Energy and Exergy Study of Effective Parameters on Performance of Photovoltaic/Thermal Natural Air Collectors, Journal of Solar Energy Engineering, 136 (2014) 031001-031001-031011.

[19] I. Guarracino, A. Mellor, N.J. Ekins-Daukes, C.N. Markides, Dynamic coupled thermal-and-electrical modelling of sheet-and-tube hybrid photovoltaic/thermal (PVT) collectors, Applied Thermal Engineering, 101 (2016) 778-795.

[20] P. Talebizadeh, M.A. Mehrabian, M. Abdolzadeh, Prediction of the optimum slope and surface azimuth angles using the genetic algorithm, Energy and buildings, 43 (2011) 2998-3005.

[21] S.A. Keshavarz, P. Talebizadeh, S. Adalati, M.A. Mehrabian, M. Abdolzadeh, Optimal slope-angles to determine maximum solar energy gain for solar collectors used in Iran, International Journal of Renewable Energy Research (IJRER), 2 (2012) 665-673.

[22] T. Tsuji, Y. Nagano, Characteristics of a turbulent natural convection boundary layer along a vertical flat plate, International journal of heat and mass transfer, 31 (1988) 1723-1734.

[23] R.W. Fox, A.T. McDonald, P.J. Pritchard, Introduction to fluid mechanics, John Wiley & Sons New York, 1998.

[24] A. Shahsavar, M. Salmanzadeh, M. Ameri, P. Talebizadeh, Energy saving in buildings by using the exhaust and ventilation air for cooling of photovoltaic panels, Energy and buildings, 43 (2011) 2219-2226.

[25] S. Klein, Calculation of flat-plate collector loss coefficients, Solar Energy, 17 (1975) 79-80.

[26] J.A. Duffie, W.A. Beckman, Solar engineering of thermal processes, John Wiley & Sons, 2013.

[27] K. Hollands, T. Unny, G. Raithby, L. Konicek, Free convective heat transfer across inclined air layers, Journal of Heat Transfer, 98 (1976) 189-193.

[28] A.A. Hegazy, Comparative study of the performances of four photovoltaic/thermal solar air collectors, Energy Conversion and Management, 41 (2000) 861-881.

[29] K. Randall, J. Mitchell, M. El-Wakil, Natural convection heat transfer characteristics of flat plate enclosures, Journal of Heat Transfer, 101 (1979) 120-125.

[30] H.S. Rauschenbach, Solar cell array design handbook: the principles and technology of photovoltaic energy conversion, Springer Science & Business Media, 2012.

[31] T. Bergene, O.M. Løvvik, Model calculations on a flat-plate solar heat collector with integrated solar cells, Solar Energy, 55 (1995) 453-462.

Corresponding Author: **Sirous Yasseri**, Tel: +44 115 823 2000, Fax: +44 115 823 2000, E-mail: sirous.yasseri@Brunel.ac.uk